

NOTES AND CORRESPONDENCE

**Predictability of the Downward Migration of
the Northern Annular Mode: A Case Study for January 2003****Hitoshi MUKOUGAWA***Disaster Prevention Research Institute, Kyoto University, Uji, Japan*

and

Toshihiko HIROOKA*Department of Earth and Planetary Sciences, Kyushu University, Fukuoka, Japan**(Manuscript received 10 April 2007, in final form 18 July 2007)***Abstract**

The dynamics and predictability of a downward migration event of the negative Northern Annular Mode (NAM) anomaly following a stratospheric sudden warming (SSW) occurring in January 2003 are examined using the operational 1-month ensemble forecast data set provided by the Japan Meteorological Agency. It is found that the predictable period of the tropospheric negative NAM anomaly is at most 6 days, which is much shorter than that of the precedent SSW event. The tropospheric NAM anomaly is caused by the E-P flux convergence associated with zonal wavenumber 2 planetary waves at the tropopause level, of which propagating property is affected by the zonal-mean zonal wind there. Our results suggest that even large stratospheric circulation changes associated with the SSW event have only limited influence on the predictability of the tropospheric circulation.

1. Introduction

Recent studies have revealed that the understanding of the downward influence of the stratospheric circulation change on the troposphere is important to improve the forecast skill of the extended-range predictions. In particular, the Northern Annular Mode (NAM) corresponding to the dominant mode of the extratropical atmosphere is considered to be a key component to understand such downward influence of the stratosphere due to its downward migration characteristics revealed by Baldwin and Dun-

kerton (1999, 2001). Baldwin et al. (2003) proposed a statistical method to predict the monthly-mean Arctic Oscillation (AO) signature in the lower atmosphere using the preceding NAM index in the lower stratosphere. The AO signature is identical to the NAM index at 1000 hPa. Since the variation of the predicted AO signature based on the preceding NAM index at 150 hPa is larger than that based on the preceding AO signature, they insisted on the validity of the proposed statistical method to predict the AO signature. However, the practical limit of the predictability of the AO signature associated with the downward migration of the NAM has not been revealed using operational extended-range numerical prediction results.

On the other hand, our recent works [Mukou-

Corresponding Author: Hitoshi Mukougawa, Disaster Prevention Research Institute, Kyoto University, Gokasho, Uji, 611-0011, Japan.
E-mail: mukou@dpac.dpri.kyoto-u.ac.jp
© 2007, Meteorological Society of Japan

gawa and Hirooka 2004 (hereafter M04); Mukougawa et al. 2005 (hereafter M05)] indicated the prolonged predictability of stratospheric circulation during stratospheric sudden warming (SSW) events up to 1 month using the Japan Meteorological Agency (JMA) 1-month prediction results. The prolonged predictability is associated with the long timescale inherent to the planetary waves propagating upward from the troposphere before the SSW events. Moreover, since the stratospheric circulation during the SSW events is characterized by negatively large NAM anomalies that descend gradually, we could expect prolonged predictability of negative AO events after SSW episodes. Thus, in this study, we will examine the dynamics and the predictability of downward migration of negative NAM anomalies observed in January 2003 just after a SSW event using all members of the JMA 1-month ensemble prediction results. We will also try to reveal the precursory event for the downward migration of the negative NAM anomaly to the troposphere.

2. Data and analysis method

We used operational ensemble 1-month (34-day) forecast data sets provided by the JMA from November 2003 to January 2004. The JMA ensemble 1-month prediction has been carried out at 1200 UTC every Wednesday and Thursday with 12 perturbed and 1 unperturbed initial conditions. Numerical integrations are conducted using a JMA global spectral model (JMA-GSM0103) with triangular 106 truncation (T106) and 40 vertical levels up to 0.4 hPa. For further model details, the reader should refer to M05. The initial perturbations are obtained using the Breeding of Growing Modes (BGM) method (Toth and Kalnay 1993). The forecast data have been archived every 24 h for the 34-day prediction period on a $2.5^\circ \times 2.5^\circ$ longitude-latitude grid at 22 levels from 1000 to 1 hPa. To verify model forecasts, JMA Global Analyses data set with 1.25-degree horizontal resolution at 23 levels from 1000 to 0.4 hPa is used.

As in M04, we also used the operational ECMWF twice-daily data set during 1985–2001 with 2.5-degree horizontal resolution at 14 levels from 1000 to 10 hPa to obtain the NAM index by the following procedure. First, the seasonal cycle, averaged over 17 years and

subject to 5-day running average, is removed from the daily geopotential height on each grid-point to define height anomalies. After applying a 10-day low-pass filter (Blackmon 1976) to the anomalies, we perform a combined EOF analysis, which combines geopotential height field at 50, 500, and 1000 hPa levels as in Yamazaki and Shinya (1999) to the low-pass filtered wintertime (November–April) anomalies. The analysis domain is poleward of 20°N , and the grid data are weighted by the square root of the cosine of latitude as well as the square root of density at each level. The leading combined EOF mode corresponding to the NAM accounts for 11.3% of the total variance. Then, the regression map ψ_l for geopotential height at each level l corresponding to anomaly values associated with one standard deviation of the leading principal component is used to define the NAM index $NAM_l(t)$ at level l as follows:

$$NAM_l(t) = \frac{(\mathbf{Z}\mathbf{A}_l(t) \cdot \boldsymbol{\psi}_l)}{(\boldsymbol{\psi}_l \cdot \boldsymbol{\psi}_l)}, \quad (1)$$

where $\mathbf{Z}\mathbf{A}_l(t)$ denotes the daily anomaly field at level l and $(\mathbf{a} \cdot \mathbf{b})$ indicates an inner product of the vectors \mathbf{a} and \mathbf{b} taking account of the areal dependence on the latitude.

3. Results

3.1 Predictability of the negative AO event

During January 2003, a warming episode took place in the Northern Hemisphere stratosphere (Fig. 1), corresponding to a negatively large NAM event in the stratosphere. The SSW was caused by the amplification of zonal wavenumber (WN) 1 components. After the SSW, the negative NAM anomaly migrates downward within the stratosphere behind the zonal wind deceleration before 21 January. In order to analyze the dynamics of the downward migration, the zonal-mean zonal wind acceleration averaged over 50°N – 70°N is also shown in the bottom panel of Fig. 1. The deceleration at 10 hPa around 15 January is associated with the SSW due to the amplified WN 1 component. The deceleration extends down within the stratosphere accompanied with the downward migration of the NAM index before 18 January. The gradual downward migration of the deceleration is confined within the stratosphere, whereas the zonal wind concurrently decelerates over the entire troposphere around 18 Jan-

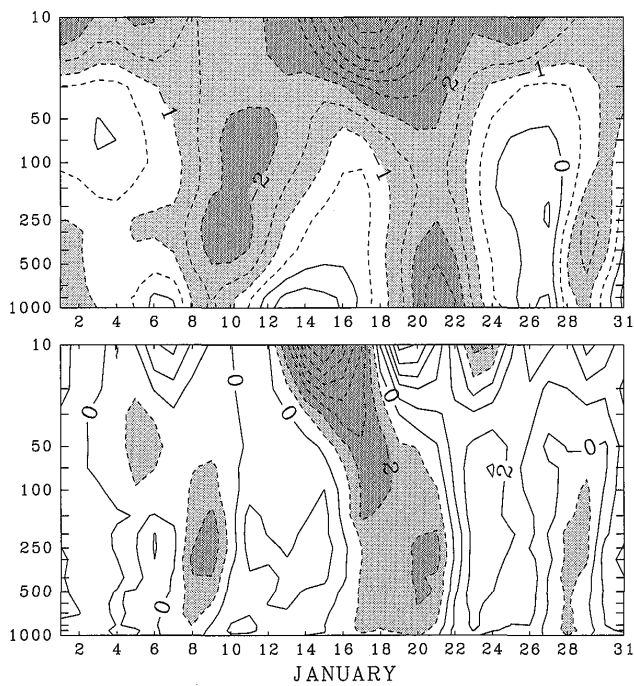


Fig. 1. Time-height [pressure (hPa)] cross section of the observed NAM index in January 2003 (upper panel), and the observed U acceleration ($\text{m s}^{-1}\text{day}^{-1}$) averaged over 50°N – 70°N . Shaded lightly (heavily) are where values are smaller than -1 (-2).

uary. Thus, the downward migration of the NAM index during this period changes its characteristics around the tropopause, consistent with the composite analysis by Baldwin and Dunkerton (1999).

In order to examine the predictability of the SSW by the JMA 1-month ensemble forecast, the time variation of observed and predicted zonal-mean temperature at 80°N and 10 hPa during January 2003 is shown in Fig. 2. For the forecasts starting from 1 and 2 January, all the ensemble members failed in predicting the occurrence of the SSW, whereas those from 8 and 9 January made successful predictions. Therefore, the SSW event is predictable more than 10 days in advance. This predictable period is somewhat shorter than that of the SSW in December 2001 reported by M05. It should be noted that the spread between the members starting from 15 and 16 January (Fig. 2c) is very small compared with those in Figs. 2a and 2b.

On the other hand, Fig. 3 shows the observed and the predicted NAM index at 1000 hPa (the

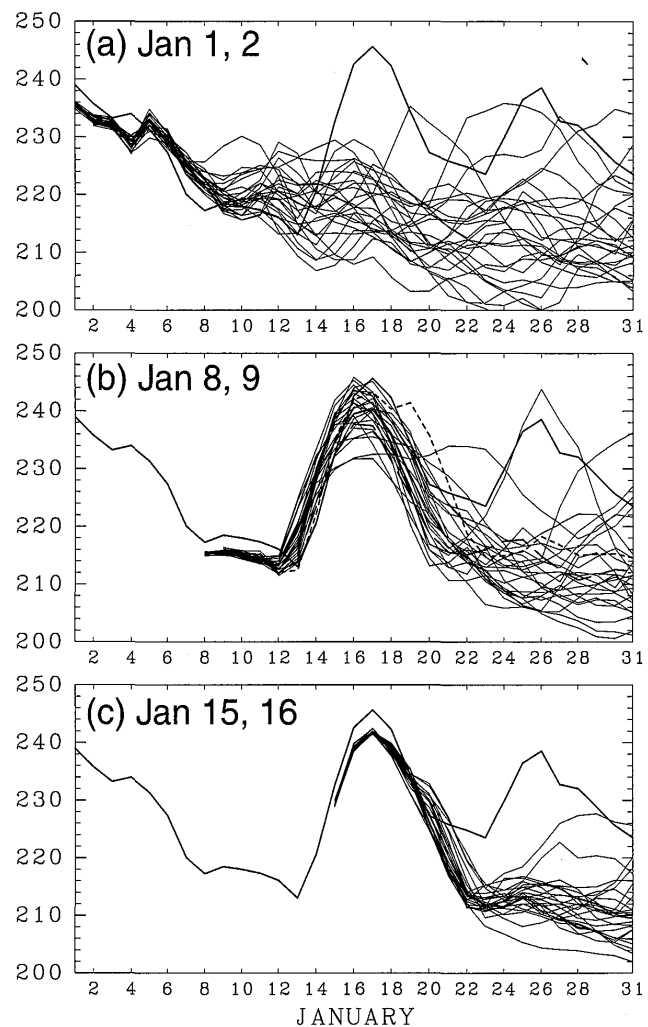


Fig. 2. Time variation of the zonal-mean temperature (K) at 80°N and 10 hPa in January 2003 for the observation (thick solid lines) and the JMA ensemble forecasts (thin solid lines) starting from 1 and 2 January (a), 8 and 9 January (b), and 15 and 16 January 2003 (c). The dotted and broken lines in (b) coincide with run A and run B in Fig. 3, respectively. As regards run A and run B, see the text.

AO signature). In the following, we will focus on the negative AO event around 21 January just after the SSW. For the forecasts starting from 1 and 2 January, which failed in predicting the SSW, the spread of the predicted AO signature around 21 January is too large to discuss the predictability of the negative AO event (Fig. 3a). The ensemble members starting from 8 and 9 January, which succeeded in predicting the SSW, also have a large spread for the AO

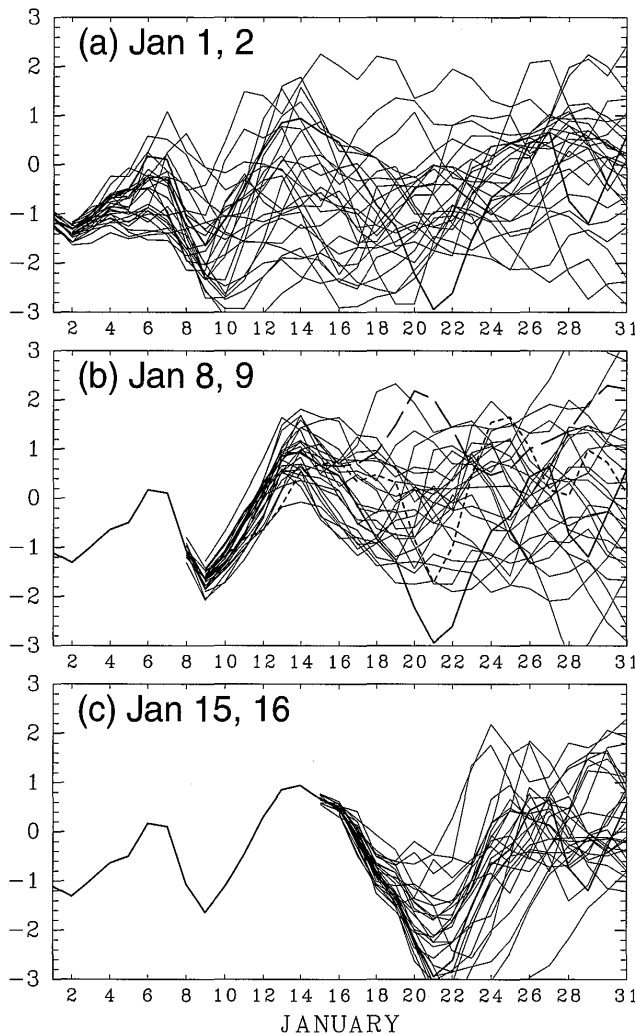


Fig. 3. As in Fig. 2, but for AO signature.

prediction (Fig. 3b). In fact, some members predict a positive AO signature just after the SSW event. Moreover, although all the members starting from one week after (Fig. 3c) predict negative AO signatures around 21 January, the spread of the predicted AO signature is still large. Thus, it is found that the predictable period of the negative AO event is at most 6 days, which is much shorter than that of the precedent SSW event.

3.2 Dynamical processes related to the negative AO event

In order to reveal the influence of the stratospheric circulation to the prediction of the negative AO event after the SSW, we will examine the ensemble prediction starting from 8 and 9 January in detail (Fig. 3b). At first, we will compare the best (run A; the dotted line) and

the worst forecast (run B; the broken line) for the prediction of the negative AO event among the ensemble members. The predicted AO signature by run A (run B) attains the minimum (maximum) value on 21 January among the ensemble members. The analysis based on the transformed Eulerian mean equation reveals that the E-P flux convergence associated with WN 2 components plays a dominant role in the zonal wind deceleration poleward of 50°N in the troposphere as well as in the stratosphere after the SSW (not shown).

Figure 4 shows the time-height cross section of the zonal wind acceleration (left panels) and the E-P flux convergence of WN 2 (right panels) for the observation (Fig. 4a), run A (Fig. 4b), and run B (Fig. 4c). Run A well reproduces the downward migration of the negative NAM anomaly into the troposphere, while such a feature is significantly weak for run B. For the observation, the convergence of WN 2 E-P flux becomes evident around 18 January in the lower stratosphere accompanied with the downward migration of the deceleration region. The convergence of WN 2 E-P flux in the upper troposphere also becomes distinct around the same period. This suggests that the downward migration of the negative NAM anomaly is associated with the coincident occurrence of the convergence of WN 2 E-P flux in the troposphere and the stratosphere. Run A (Fig. 4b) well reproduces the dominant convergence of WN 2 E-P flux similar to the observation although the magnitude is smaller than the observation. However, run B (Fig. 4c) does not simulate the convergence in the troposphere at all, although the convergence in the stratosphere is well reproduced. Therefore, it is necessary to well simulate the behavior of WN 2 planetary waves in the upper troposphere for the prediction of the downward migration of the negative NAM anomaly into the troposphere.

Then, we investigated the characteristic of WN 2 planetary waves over a 3-day period from 18 to 20 January, when the zonal wind deceleration becomes evident. Figure 5 shows the E-P flux vector and the associated convergence averaged over the 3-day period. For the observation (Fig. 5a), the upward propagation of WN 2 components concentrates around 50°N in the troposphere, and there is strong convergence of the E-P flux in the poleward region of

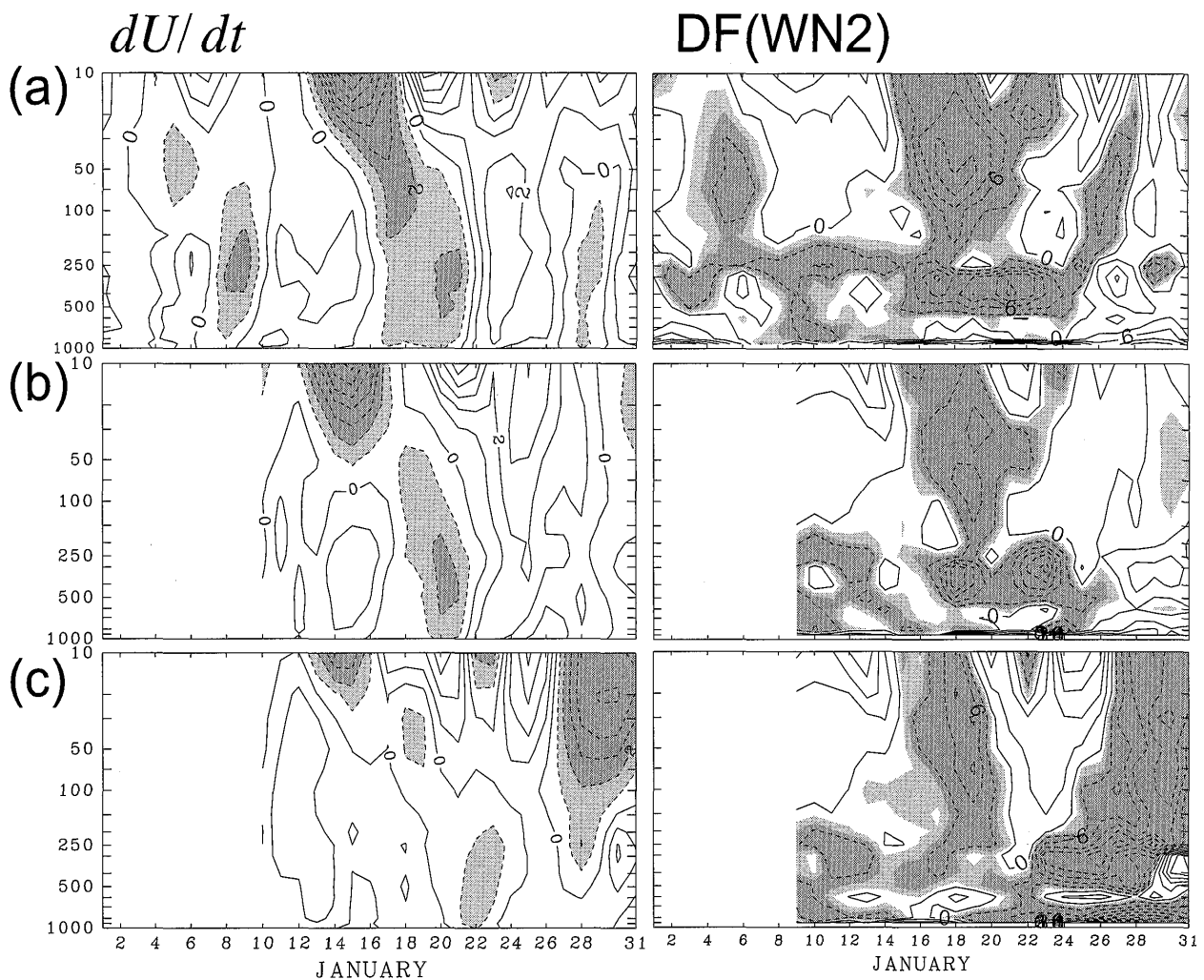


Fig. 4. Time-height [pressure (hPa)] cross section for the U acceleration (dU/dt) (left panels), and the zonal force per unit mass $(\rho_0 a \cos \phi)^{-1} \nabla \cdot \mathbf{F}$ associated with WN 2 E-P flux \mathbf{F} (right panels) in January 2003. Both values are averaged over 50°N – 70°N and the unit is $\text{m s}^{-1}\text{day}^{-1}$. Shaded lightly (heavily) are where values are smaller than -1 (-2) $\text{m s}^{-1}\text{day}^{-1}$. (a) The observation, (b) run A, and (c) run B.

the upper troposphere. The wave activity further propagates upward and poleward in the stratosphere, and converges in the middle stratosphere. Run A (Fig. 5b) has a somewhat weaker wave activity than the observation, and the upward propagating region shifts poleward. The convergence of the E-P flux in the upper troposphere is still evident as in the observation. However, for run B (Fig. 5c), the convergence of the E-P flux is considerably weak, and the wave activity tends to propagate equatorward in the upper troposphere, in contradiction to the observation and run A. A clear difference in the geopotential height distribution in the troposphere is also seen during this period (not shown). A dominant blocking high

resides over Alaska for run A and the observation, while the blocking has already faded away through downstream energy dispersion for run B. Moreover, the trough over the north Pacific for run A and the observation has the southeast to northwest phase tilt, while that for run B has the opposite meridional phase tilt. This is consistent with the difference in the direction of the meridional propagation of the WN 2 component as seen in Fig. 5.

To further examine the propagating property of WN 2 planetary waves during this period, the zonal-mean zonal wind (U) distribution during this period is shown in the upper panels of Fig. 6. Westerlies in the high latitude of stratosphere and troposphere for run B (Fig.

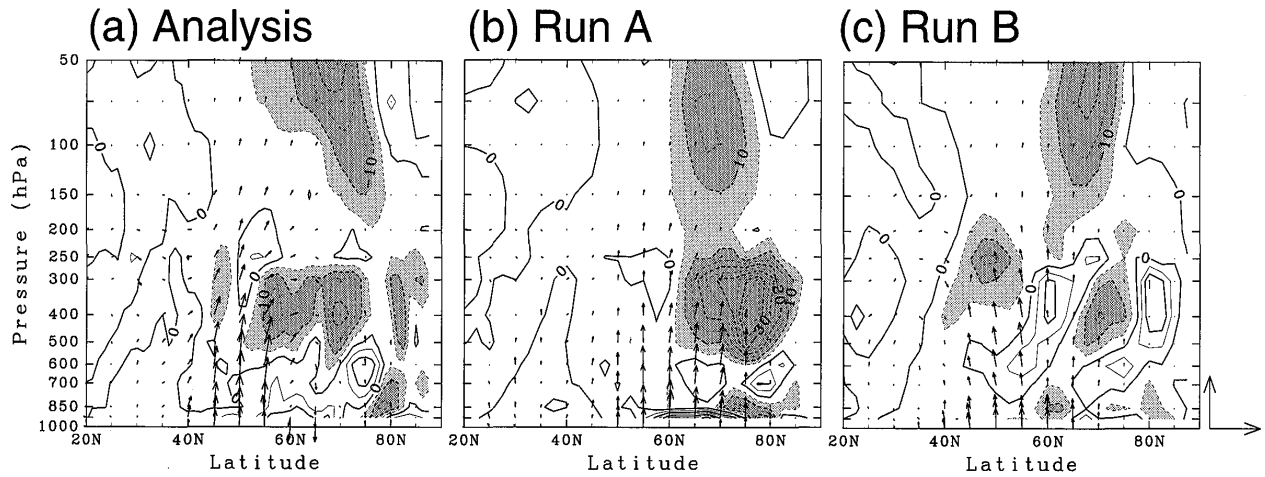


Fig. 5. Latitude-height cross sections for the time-mean WN 2 E-P flux F (arrows; kg s^{-2}) and the associated zonal force per unit mass $(\rho_0 a \cos \phi)^{-1} \nabla \cdot F$ (contours; $\text{m s}^{-1} \text{day}^{-1}$) averaged over 18–20 January 2003. (a) The observation, (b) run A, and (c) run B. Arrows in the right bottom correspond to $(4.0 \times 10^8, 1.5 \times 10^6)$. Shaded lightly (heavily) are where values are smaller than -5 (-10) $\text{m s}^{-1} \text{day}^{-1}$.

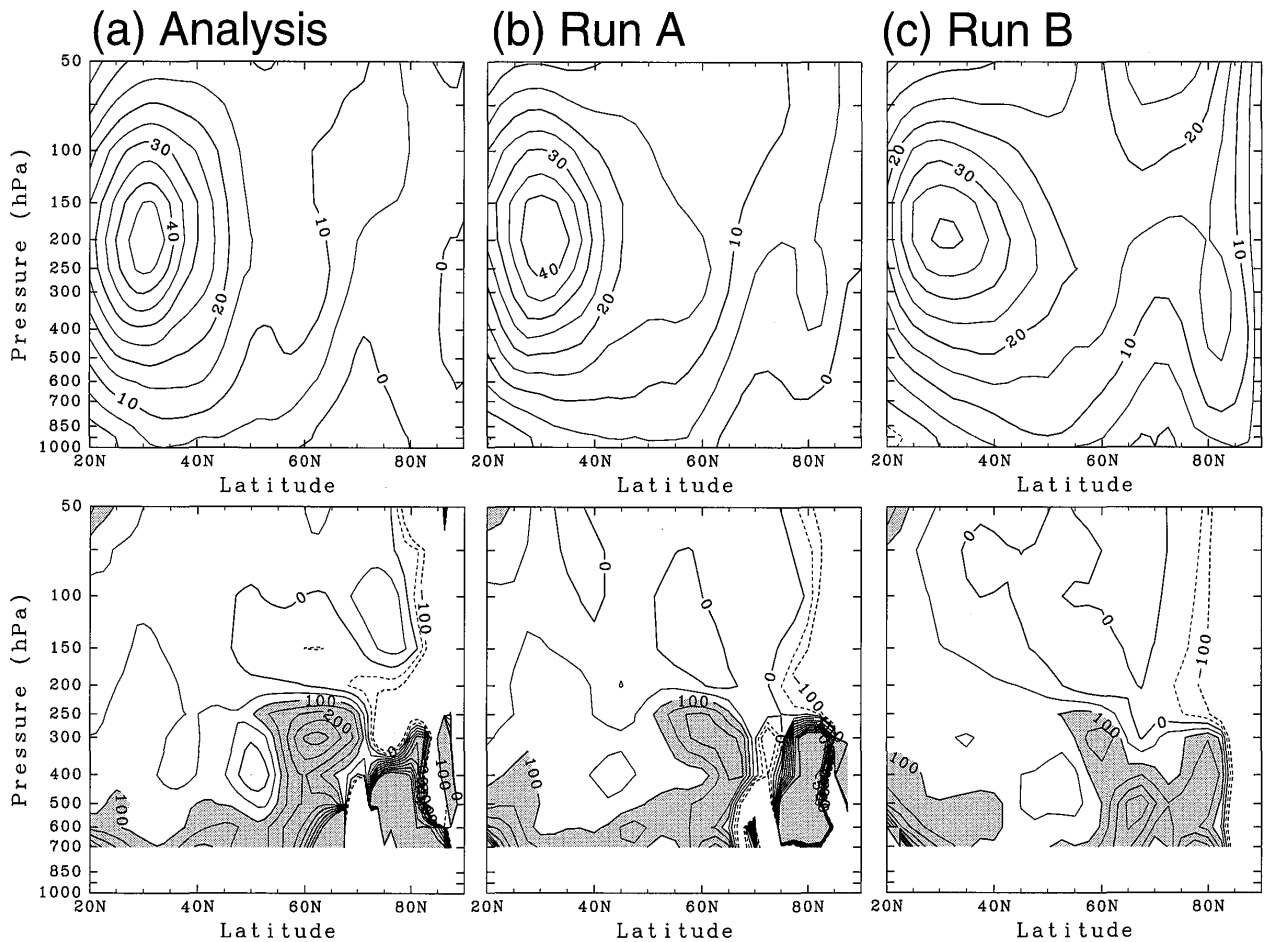


Fig. 6. As in Fig. 5, but for U (upper panels; m s^{-1}) and the corresponding refractive index squared n^2 in Eq. (2) for the stationary WN 2 component multiplied by a^2 the square radius of the earth (lower panels). Values larger than 100 are shaded, and contours with values larger than 500 or smaller than -100 are omitted in the lower panels.

6c) are stronger than those for the observation (Fig. 6a) and run A (Fig. 6b). Run B is also characterized by a comparatively weaker subtropical jet core expanding poleward. The lower panels in Fig. 6 show the corresponding refractive index squared n^2 (Andrews et al. 1987; Lorenz and Hartmann 2003) for stationary WN 2 ($k = 2$) defined by

$$n^2 = \frac{\bar{q}_\phi}{U} - \left(\frac{k}{a \cos \phi} \right)^2 - \left(\frac{f}{2NH} \right)^2. \quad (2)$$

Here, we use the log-pressure coordinate ($z = -H \ln(p/p_s)$), and ϕ is the latitude, a the radius of the earth, f the Coriolis parameter $f \equiv 2\Omega \sin \phi$ where Ω is the earth's rotation rate, N the log-pressure buoyancy frequency [Eq. (3.2.13) in Andrews et al. 1987], H the scale height, \bar{q}_ϕ the meridional gradient of the zonal-mean quasi-geostrophic potential vorticity defined as

$$\bar{q}_\phi = \frac{2\Omega}{a} \cos \phi - \frac{1}{\alpha^2} \left\{ \frac{(U \cos \phi)_\phi}{\cos \phi} \right\}_\phi + \frac{f^2}{N^2} \left((\ln N^2)_z + \frac{1}{H} \right) U_z - \frac{f^2}{N^2} U_{zz}. \quad (3)$$

Figure 6 indicates that a distinctive maximum of the refractive index squared n^2 exists for the observation and run A around 300 hPa and 60°N, while the maximum region is obscure for run B. By examining each term in Eq. (2), it is found that the maximum region of n^2 in the observation as well as run A is caused by $U_{zz} < 0$ there, consistent with the fact that U attains a local maximum in the tropopause region as seen in the upper panels of Fig. 6. Figure 6 also reveals that the poleward propagation in the upper troposphere around 50°N as seen in Fig. 5 is associated with the maximum n^2 region around 60°N. Therefore, it is suggested that the slight difference in the U profile in the tropopause region significantly affects the propagating property of the WN 2 component in the upper troposphere. On the contrary, the difference of n^2 in the lower stratosphere is not so evident. The evanescent region with negative n^2 prevails in the midlatitudes for the observation and run A as well as run B.

The possible relationship between the characteristic U profile and the subsequent occurrence of the negative AO event as seen in Fig. 6 is also confirmed by the regression analysis

on U using all ensemble members (26) of the forecast starting from 8 and 9 January as in M05. Figure 7b shows U anomalies (U_A) averaged over 18–20 January associated with a negative one-standard deviation anomaly of the AO signature on 21 January. Here, the anomaly is defined as the deviation from the ensemble mean (Fig. 7a). For the ensemble mean field (U_M), relatively strong westerlies are seen in the polar region, and the poleward propagation of WN 2 E-P flux is not so evident, in common with run B (Fig. 6c). Statistical significance of the correlation is also assessed by Student's t -test based on 24 degrees of freedom, and shown by shades in Fig. 7b. From this figure, we confirm that the easterly anomaly around 60°N along with the westerly anomaly in the subtropical jet core region is significantly related to the following occurrence of the negative AO signature. Figure 7b also shows the significant E-P flux anomaly of the WN 2 component, which has an enhanced activity in the troposphere and tends to propagate upward and poleward around 60°N. Since the U_A regression pattern shown in Fig. 7b has large projection on to the negative AO event, the U_A pattern indicates the direction to the negative AO event in phase space, and the associated E-P flux anomalies represent the developing mechanism of the negative AO event. The two separate regions with anomalously enhanced E-P flux convergence are seen around the 50-hPa level and the tropopause region (Fig. 7c). This fact suggests that the framework of the gradual downward migration of the negative NAM index from the stratosphere to the lower troposphere is not appropriate for this negative NAM event. Rather, the zonal winds in the troposphere decelerate concurrently with those in the stratosphere.

Figure 8 shows the distribution of the refractive index squared n^2 for the stationary WN 2 component accompanied with the U profile for the ensemble mean U_M (Fig. 7a), $U_M + U_A$ (Fig. 7b), and $U_M - U_A$ (Fig. 7c). It is found that n^2 becomes large (small) in the high latitude at the tropopause region with the positive (negative) zonal wind anomaly of Fig. 7b, i.e., U_A ($-U_A$). The vertical curvature term U_{zz} in Eq. (3) plays a dominant role in creating the anomalously large n^2 in the tropopause region. The large n^2 region would also promote the

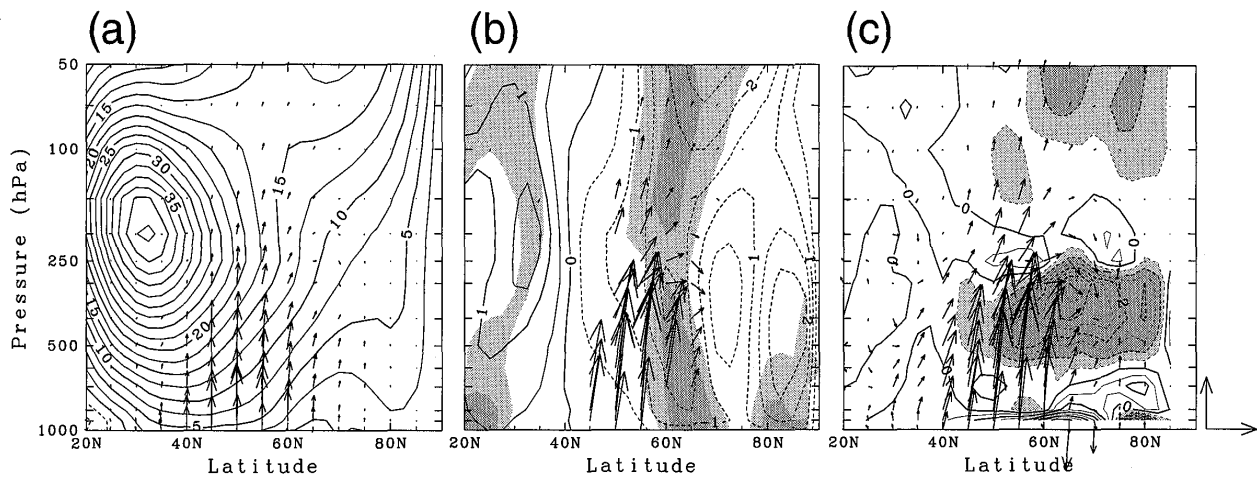


Fig. 7. (a) Ensemble mean U_M of the predicted U (contours; m s^{-1}) along with the WN 2 E-P flux (arrows; kg s^{-2}) averaged over 18–20 January 2003. The magnitude of the vector is multiplied by 0.1. (b) As in (a), but for regressed negative anomaly U_A of the predicted 3-day averaged U (m s^{-1}) during 18–20 January with respect to the predicted AO signature on 21 January. The light (heavy) shades indicate regions where the statistical significance of the anomaly exceeds 95 (99)%. The regressed WN 2 E-P flux anomalies F (kg s^{-2}) of which vertical components are significant at the 95% level are also shown. (c) As in (b), but for the zonal force per unit mass ($\text{m s}^{-1}\text{day}^{-1}$) associated with F in (b). Contour interval is 0.5, and values larger than 0.5 (1.0) are lightly (heavily) shaded. Arrows in the right bottom correspond to $(2.0 \times 10^7, 5.4 \times 10^4)$.

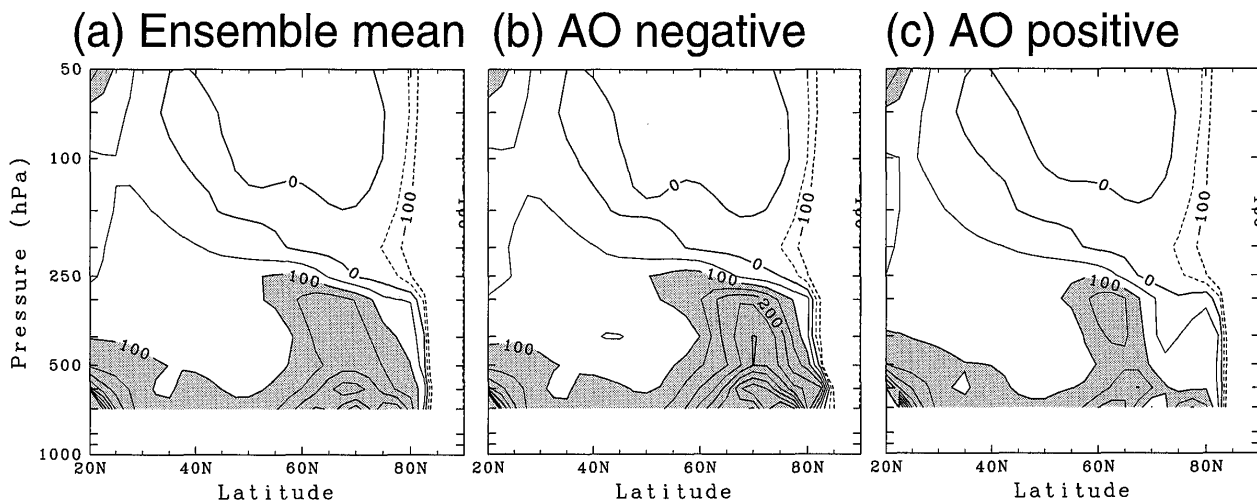


Fig. 8. Refractive index squared n^2 of the stationary WN 2 component multiplied by a^2 . The U profile for (a) is given by U_M , while those for (b) and (c) are specified by $U_M + U_A$ and $U_M - U_A$, respectively. Values larger than 100 are shaded, and contours with values larger than 500 or smaller than -100 are omitted.

poleward propagation of WN 2 component, as seen in Fig. 7c. On the other hand, the n^2 profile in the lower stratosphere is similar to each other for the three panels in Fig. 8, which suggests that the regressed U anomaly in the

lower stratosphere is not important to modulate the propagating property of WN 2 component during this period. Thus, the regression analysis using all ensemble members also suggests the important role of the U anomaly

around the tropopause region for the subsequent occurrence of the negative NAM event over the entire troposphere. The tropospheric WN 2 waves might be responsible for the tropopause U anomaly shown in Fig. 7b since the E-P flux convergence of WN 2 component is already evident after 16 January as seen in Fig. 4a.

4. Concluding remarks

We examined the dynamics and the predictability of a downward migration event of the negative NAM anomaly occurring in January 2003 just after a SSW by the use of all ensemble members of the 1-month forecasts performed by the JMA. It was found that the E-P flux convergence associated with the WN 2 component plays a dominant role for the downward migration of the negative NAM anomaly, while the SSW is caused by the amplification of the WN 1 component. The predictable period of the negative NAM anomaly in the troposphere is 6 days at most, and the ensemble members that succeeded in predicting the occurrence of the SSW do not necessarily well predict the following negative NAM anomaly in the troposphere. Thus, the predictability of the negative NAM anomaly in the troposphere is quite limited compared with that of the SSW.

In this study, we have argued on the dynamical predictability of daily variation of the AO index after the SSW, while Baldwin et al. (2003) discussed the statistical predictability of the monthly-mean AO index. Hence, it might be plausible to think that the time averaged AO index has an improved forecast skill compared with the daily index. However, the time averaging procedure does not necessarily improve the forecast skill on the basis of the present case study. This can be seen from Fig. 3b. After 16 January, the observed AO index tends to be negative (time averaged AO index for the period from 16 to 31 January is -0.79), while the time average of the ensemble-mean prediction of the AO index is 0.06 for the same period. Of course, we have to conduct more detailed analysis on the dynamical predictability of the monthly-mean AO index using seasonal forecast datasets for a further study.

It is also revealed that the fair reproduction of WN 2 planetary waves propagating upward and poleward from the troposphere into the

stratosphere is important for the successful prediction of the downward migration of the negative NAM anomaly. The analysis on the refractive index indicates that the tropopause zonal-mean zonal wind (U) profile rather than the stratospheric U anomaly after the SSW significantly affects the propagating property of the WN 2 component. Hence, it is suggested that the stratospheric U anomaly after the SSW can hardly affect the predictability of the tropospheric negative NAM anomaly in comparison with the tropopause U anomaly.

Of course, we have to examine other downward migration events of the negative NAM anomaly to confirm our results. Moreover, hindcast experiments using the numerical prediction model are also necessary to reveal the dynamical relationship between the tropopause U anomaly and the propagation and the generation of the WN 2 planetary waves during this period.

Acknowledgments

We would like to thank all the members in Numerical Prediction and Climate Prediction Divisions in JMA for providing us 1-month forecast data sets of JMA. This work was supported by Grant-in-Aids for Scientific Research (A) 18204043, 18204044, and (B) 15340155 from JSPS. The GFD-DENNOU Library was used for the graphics.

References

- Andrews, D.G., J.R. Holton, and C.B. Leovy, 1987: *Middle Atmosphere Dynamics*. Academic Press, 489 pp.
- Baldwin, M.P. and T.J. Dunkerton, 1999: Propagation of the Arctic Oscillation from the stratosphere to the troposphere. *J. Geophys. Res.*, **104**, 30937–30946.
- Baldwin, M.P. and T.J. Dunkerton, 2001: Stratospheric harbingers of anomalous weather regimes. *Science*, **294**, 581–584.
- Baldwin, M.P., D.B. Stephenson, D.W.J. Thompson, T.J. Dunkerton, A.J. Charlton, and A. O’Neil, 2003: Stratospheric memory and skill of extended-range weather forecasts. *Science*, **301**, 636–640.
- Blackmon, M.L., 1976: A climatological spectral study of the 500 mb geopotential height of the Northern Hemisphere. *J. Atmos. Sci.*, **33**, 1607–1623.

- Lorenz, D.J. and D.L. Hartmann, 2003: Eddy-zonal flow feedback in the Northern Hemisphere winter. *J. Climate*, **16**, 1212–1227.
- Mukougawa, H. and T. Hirooka, 2004: Predictability of stratospheric sudden warming: A case study for 1998/99 winter. *Mon. Wea. Rev.*, **132**, 1764–1776.
- Mukougawa, H., H. Sakai, and T. Hirooka, 2005: High sensitivity to the initial condition for the prediction of stratospheric sudden warming. *Geophys. Res. Lett.* **32**, L17806, doi:10.129/2005GL022909.
- Toth, Z. and E. Kalnay, 1993: Ensemble forecasting at NMC: The generation of perturbations. *Bull. Amer. Meteor. Soc.*, **74**, 2317–2330.
- Yamazaki, K. and Y. Shinya, 1999: Analysis of the Arctic Oscillation simulated by AGCM. *J. Meteor. Soc. Japan*, **77**, 1287–1298.